HHS Public Access

Author manuscript

J Struct Biol. Author manuscript; available in PMC 2022 March 16.

Published in final edited form as:

J Struct Biol. 2022 March ; 214(1): 107838. doi:10.1016/j.jsb.2022.107838.

Structural principles of CRISPR-Cas enzymes used in nucleic acid detection

Anuska Das[a,1], **Hemant N. Goswami**[a,1], **Charlisa T. Whyms**[b,1], **Sagar Sridhara**[a,2], **Hong Li**[a,b,*]

[a]Institute of Molecular Biophysics, Florida State University, Tallahassee, FL 32306, USA

[b]Department of Chemistry and Biochemistry, Florida State University, Tallahassee, FL 32306, USA

Abstract

Clustered Regularly Interspaced Short Palindromic Repeat (CRISPR)-based technology has revolutionized the field of biomedicine with broad applications in genome editing, therapeutics and diagnostics. While a majority of applications involve the RNA-guided site-specific DNA or RNA cleavage by CRISPR enzymes, recent successes in nucleic acid detection rely on their collateral and non-specific cleavage activated by viral DNA or RNA. Ranging in enzyme composition, the mechanism for distinguishing self- from foreign-nucleic acids, the usage of second messengers, and enzymology, the CRISPR enzymes provide a diverse set of diagnosis tools in further innovations. Structural biology plays an important role in elucidating the mechanisms of these CRISPR enzymes. Here we summarize and compare structures of three types of CRISPR enzymes used in nucleic acid detection captured in their respective functional forms and illustrate the current understanding of their activation mechanism.

Keywords

CRISPR-Cas enzyme structures; Nucleic acid detection; Cas12; Cas13; Csm; Cmr; Csm6; Csx1; Card1

1. Introduction

Clustered Regularly Interspaced Short Palindromic Repeat (CRISPR) and CRISPR-associated proteins (Cas) systems have immensely advanced the field of biomedicine in the past decade (Barrangou and Doudna, 2016; Zhang, 2019). Found in most archaea and many bacteria, CRISPR-Cas systems provide an adaptive immunity against bacteriophages and

*Corresponding author at: Institute of Molecular Biophysics, Florida State University, Tallahassee, FL 32306, USA. hong.li@fsu.edu (H. Li).

[1]Authors contributed equally.

[2]Current address: Department of Medical Biochemistry and Cell Biology, University of Gothenburg, Gothenburg 40530, Sweden.

Declaration of Competing Interest

The authors declare that they have no known competing financial interests or personal relationships that could have appeared to influence the work reported in this paper.

other invading predatory mobile genetic elements (MGEs) such as plasmids and transposons (Faure et al., 2019). Such an immunity is achieved in a three-stage process: adaptation to infection by incorporation of new spacers derived from MGEs, processing of CRISPR RNA (crRNA) to yield mature guide RNA and interference against target DNA/RNA by CRISPR-Cas nucleases (Barrangou, 2015; Sorek et al., 2013; Wright et al., 2016; Barrangou and Marraffini, 2014). The extraordinary programmability of the CRISPR-Cas effectors through crRNA has found convenient applications in genome editing, therapeutics and more recently, specific nucleic acid detections (Barrangou and Doudna, 2016; Zhang, 2019; Freije and Sabeti, 2021; Wang et al., 2020).

CRISPR-Cas effectors are highly diverse in composition, structures and functions (Makarova, 2020). They have been mainly categorized based upon the architecture of CRISPR effector modules: Class I comprising multi-subunit effector complexes (Makarova et al., 2017) and Class II containing single-subunit effector complexes (Makarova et al., 2017). Based on features in CRISPR loci, the effectors are also classified into six different types. Both classes of CRISPR-Cas effectors representing three different types have been repurposed towards nucleic acid detection applications. The Class II enzymes, Cas12 (Type V) and Cas13 (Type VI), have been predominantly exploited via breakthrough technologies (Freije and Sabeti, 2021) like DETECTR (Chen et al., 2018), HOLMES (Li et al., 2018), and SHERLOCK (Gootenberg et al., 2017). On the other hand, recent technologies such as MORIARTY (Sridhara et al., 2021) and SCOPE (Steens et al., 2021) employ the Class I systems (Type III) based on their inherent tandem nucleic acid cleavage activities. Regardless of the types, the CRISPR enzymes can be programmed with the ability to base pair with a specific viral nucleic acid sequence that if encountered, will stimulate *trans*-cleavage of single stranded DNA or RNA by the CRISPR enzymes (Fig. 1). This *trans*-cleavage activity is then harnessed as a reporter for the presence of the viral nucleic acids. Recent biochemical and structural studies have begun to elucidate the molecular basis for the *trans*-cleavage activity of the CRISPR enzymes in order to provide blueprints for designing and improving unique nucleic acid detection strategies. While this graphical review focuses on the mechanisms underlying the CRISPR enzyme-based diagnosis, we direct readers to other excellent comprehensive reviews on CRISPR-Cas structures (Molina et al., 2020; Stella et al., 2017; Jiang and Doudna, 2017; Swarts and Jinek, 2018).

1.1. Structural mechanism of DNA detection by Cas12

Cas12 is a Type V effector protein belonging to Class II. Most known Cas12 enzymes target double stranded (ds) DNA but recently one subtype, Cas12i, was found to target RNA (Zhang et al., 2020). To cleave the DNA substrate, Cas12 requires a region in the DNA (protospacer) complementary to its associated crRNA (spacer) and a stretch of DNA at the 5' end of the protospacer called Protospacer Adjacent Motif (PAM). Among the Cas12 family of enzymes, the most studied are Cas12a, also known as Cpf1, and Cas12b, also known as C2c1. The PAM sequence for Cas12 is mostly thymine rich and located near the 5' end of the protospacer. While Cas12a enzymes do not require the long and bulky *trans*-activating crRNA (tracrRNA) in targeting DNA, Cas12b require tracrRNA to achieve interference (Stella et al., 2017). Together with the unique features in Cas12 such as being small in size and processing own precursor CRISPR (pre-crRNA) without the need for Cas6, Cas12 has

found applications in both genome editing (Zetsche et al., 2017) and nucleic acid detection (Freije and Sabeti, 2021; Chen et al., 2018; Li et al., 2018; Li et al., 2019).

Structures of Cas12 show that it is a multi-domain protein with a bilobed architecture (Stella et al., 2017; Swarts and Jinek, 2018). The nucleic acid recognition lobe (REC) is responsible for wrapping around the heteroduplex formed between the guide RNA and the target DNA strand and the nuclease (NUC) lobe contains four domains responsible for PAM recognition and catalysis. The PAM interacting domain (PI) is positioned at the PAM element to discriminate against self-DNA that lacks the correct PAM sequence and the nuclease RuvC domain performs the actual cleavage of the DNA. Unlike Cas9 that uses both the RuvC and the HNH domains to cleave the non-target and the target DNA strand, respectively, Cas12 employs the single RuvC domain to cleave both.

Remarkably, following cleavage of the dsDNA, Cas12 is activated to cleave single stranded (ss) DNA non-specifically (Chen et al., 2018; Gootenberg et al., 2018). This is the mechanistic basis for Cas12 to be employed in nucleic acid detection. By including a ssDNA oligo flanked by a fluorophore and a quencher pair, Cas12 would cleave the ssDNA probe oligo, only in presence of a stimulatory DNA bearing both PAM and the protospacer, thereby eliciting a detectable fluorescence signal (Chen et al., 2018; Li et al., 2018; Gootenberg et al., 2018) (Fig. 1). Alternatively, the cleaved ssDNA probe can be detected using a convenient paper chromatography (Freije and Sabeti, 2021; Gootenberg et al., 2018).

To elucidate the molecular mechanism of Cas12, various biochemical and biophysical studies focused on the structural changes in Cas12 upon crRNA and target DNA binding that lead to both the dsDNA cleavage and the collateral activity. While no structure of Cas12 alone is yet available, a number of crystal and electron cryomicroscopy (cryoEM) structures of Cas12 bound with crRNA and various crRNA:DNA complexes from several organisms have been obtained (Nishimasu et al., 2017; Swarts et al., 2017; Yamano et al., 2017; Stella et al., 2018; Yang et al., 2016; Stella et al., 2017). Among these, the cryoEM study of *Francisella novicida* Cas12a (FnCas12a) captured the crRNA-bound binary complex and crRNA:DNA-bound ternary complexes in several transitional forms (Stella et al., 2018). Finally, the study with the active FnCas12a enzyme and a cleavable DNA substrate captured the form where the target strand is cleaved (Stella et al., 2017). These works show that as the crRNA:protospacer pairing increases, the REC and the PI domains continue to approach the DNA, leading to a final compaction of the FnCas12a (Fig. 2). Binding of the target DNA promotes insertion of the loop-lysine helix-loop (LKL) of the PI domain into the dsDNA, which leads to separation of the dsDNA and formation of the R-loop (Fig. 2). During this process, the REC domain is significantly reorganized (Fig. 2b) (Nishimasu et al., 2017; Swarts et al., 2017; Yamano et al., 2017; Stella et al., 2018). Importantly, the catalytic residues of the RuvC domain, Asp917 and Glu1006 of FnCas12a, remain engaged by two positively charged residues, Lys1013 and Arg918, respectively, to remain inactive (Fig. 2b). In the final ternary complex prior to cleavage, these polar interactions are disengaged via a significant rearrangement of the Lys1013-bearing loop (LBL) (Fig. 2c), freeing the catalytic residues to form the active site, possibly with metal ions (Stella et al., 2018; Stella et al.,

2017). The rearrangement in the active site after dsDNA cleavage is believed to be the molecular mechanism responsible for activation of the collateral DNase activity of Cas12a.

Crystallographic studies of *Alicyclobacillus acidoterrestris* Cas12b (AacCas12b) in both the DNA-free and DNA-bound forms illustrate a similar mechanism of nucleic acid interactions as FnCas12a (Stella et al., 2017; Yang et al., 2016). Unlike FnCas12a, however, local rearrangements involving two loops in front of the RuvC domain (Lid) were observed upon dsDNA binding, which may enable target DNA positioning (Fig. 2c). Interestingly, the AacCas12b structures further show that the target and the non-target DNA strand can be alternatingly placed into the RuvC catalytic site for cleavage (Fig. 2c). The indiscriminate binding of either the target or the non-target DNA implies the possibility that non-specific ssDNA may also be able to compete with the dsDNA substate for the RuvC active site, leading to its dsDNA-activated collateral activity.

1.2. Structural mechanism of RNA and DNA detection by Cas13

Cas13 is a member of the Type VI system and also belongs to Class II. Cas13 is the first known RNA cleavage effector among the Class II enzymes and employs the Higher Prokaryotic and Eukaryotic binding domain (HEPN) as the nuclease for target RNA cleavage (Abudayyeh, 2016). The target RNA must bear a stretch of sequence complementary to the guide region of the crRNA associated with Cas13 and in addition, its 3' protospacer flanking sequence (PFS) region should not fully pair with the 5' tag of the crRNA, as pairing of these two regions inhibits cleavage (Abudayyeh, 2016; Smargon et al., 2017; Cox et al., 2017).

Similar to Cas12, Cas13 possesses target-activated collateral activity that degrades single stranded RNA non-specifically. This is the basis for Cas13a, Cas13b and more recently, Cas13d, to be used in various diagnostic applications such as SHERLOCK (Gootenberg et al., 2017), CARMEN (Ackerman et al., 2020), SHINE (Arizti-Sanz et al., 2020). By including a short RNA oligo flanked by a fluorophore and quencher pair in a Cas13-mediated reaction, cleavage of the fluorescently labeled RNA probe oligo following target RNA cleavage would lead to separation of the fluorophore and quencher, and therefore, a rise in fluorescent signal (Fig. 1). Alternatively, the cleaved RNA probe can also be detected using convenient paper chromatography (Freije and Sabeti, 2021; Abudayyeh et al., 2019).

Various structural studies of Cas13a systems from *Leptotrichia shahii* (LshCas13a), *Leptotrichia buccalis* (LbuCas13a), *and Lachnospiraceae bacterium* (LbaCas13a) have unveiled the conformational changes in Cas13a upon crRNA binding (Liu et al., 2017; Liu et al., 2017; Knott et al., 2017), and in the case of LbuCas13a, target RNA binding (Liu et al., 2017). Like Cas12, Cas13a also contains a bilobed architecture with a REC and a NUC lobe linked by a Linker domain. The NUC lobe contains two HEPN domains (HEPN1 and HEPN2) for target as well as non-specific RNA cleavage (Fig. 3a). The REC lobe contains three helixrich domains responsible for recognition of the guide RNA hairpin loop and the crRNA-target RNA helix (Fig. 3b, c & d). In the target-bound ternary complex structure, 3' PFS is observed to be at the cleft between Helical-1 and the N-terminal domain (NTD) (Liu et al., 2017; Liu et al., 2017). Binding of a cognate target RNA to LbuCas13 brings the two HEPN domains together to form a combined catalytic site (Fig.

3b, 3c & 3d). If the 3' PFS would form base pairs with the crRNA, on the other hand, as illustrated in the structure of a non-cognate target-bound LshCas13a complex (Wang et al., 2021), the domain motions involving HEPN2 would be inhibited, preventing formation of a cleavage compatible structure. The target RNA-induced structural transitions form the basis for activation of the RNase activity in Cas13 (Liu et al., 2017). Similar activation mechanism applies to Cas13d as illustrated in its target-free and target-bound structures of *Eubacterium siraeum* Cas13d (EsiCas13d) (Zhang et al., 2018), although Cas13d does not seem to require 3' PFS and has a different domain architecture (Fig. 3a). Upon cognate target RNA binding, the two HEPN domains compact to form the RNA cleavage site (Fig. 3e, f, & g).

Interestingly, the activated composite HEPN center does not cleave target RNA at specific sites. Rather, it cleaves the target RNA non-specifically at a region rich in uridine but distant to the crRNA:target pairing region (Abudayyeh et al., 2017; East-Seletsky et al., 2016). This may be achieved by the RNase activity exerted in *trans* owing to the surface exposed catalytic site. The *trans*-cleavage activity is the basis for Cas13 to be used in nucleic acid detections (Figs. 1 & 3).

1.3. Structural mechanism of RNA and DNA detection by Type III systems

The ability to re-engineer Type III systems towards the detection of nucleic acids has been demonstrated in recent studies towards diagnosing SARS-CoV-2, either by employing a Csm-Csm6 system (Sridhara et al., 2021; Santiago-Frangos et al., 2021), a Cmr-TTHB144 system (Steens et al., 2021) or a Cmr-NucC hybrid system (Gruschow et al., 2021). This application depends on the viral RNA-stimulated dual collateral activities in these Type III systems (Figs. 4 & 5). In absence of any target RNA (apo) or upon binding of the self-RNA (non-cognate target RNA, or NTR), Type III effectors remain inactive while in presence of a viral RNA (cognate target RNA, or CTR), they elicit both cyclic oligoadenylate (cOA) synthesis and deoxyribonuclease (DNase) activities in their Csm1 (Csm) or Cmr2 (Cmr) catalytic subunit (You et al., 2019; Jia, 2019; Sridhara et al., 2021; Niewoehner et al., 2017; Sofos, 2020). The cOA molecules act as second messenger in activating the ancillary ribonuclease (RNase) Csm6 (Csm) or Csx1 (Cmr) or the deoxyribonuclease NucC (Cmr) by binding to the CARF (CRISPR-associated Rossmann Fold) sensor domain (Sridhara et al., 2021; Athukoralage and White, 2021; Kazlauskiene et al., 2017). The tandem nuclease strategy is not limited to Type III-based detection systems. The ability for Cas13a to release a linear polyadenylate oligo through the primary activation was used to activate Csm6, making the Cas13-Csm6-based detection more powerful (Gootenberg et al., 2018; Liu et al., 2021). Several structures that represent the various functional forms have been obtained, allowing the comparison of the active sites, and therefore, elucidation of the mechanism of activation. We show in Fig. 4a collection of apo, NTR- and CTR-bound Csm structures from *Lactococcus lactis* (LlCsm) used in MORIARTY (Sridhara et al., 2021) and compare both the cOA_6 synthesis (GGDD motif) and DNase (HD domain) centers in these functional forms (Sridhara et al., 2021). While the cOA_6 synthesis center experience noticeable opening as a result of CTR binding that can activate cOA_6 production (Fig. 4c), minor changes are observed in the HD center regardless of whether the target RNA is bound (Fig. 4d). This conclusion also holds true to structural studies of the thermophilic *Streptococcus thermophilus* and *Thermococcus onnurineus* Csm complexes (You et al., 2019; Jia, 2019).

Authors of these studies hypothesize that CTR binding to Csm could alter protein dynamics of the catalytic subunit Csm1, through changes in other subunits and Csm1 loops, and thus activate its non-specific DNase activity. This hypothesis has found support in a single molecule fluorescence microscopy study of the *Staphylococcus epidermidis* Csm system (SeCsm) (Wang et al., 2019) and the fact that stand-alone Csm1 subunit is a constitutive DNase (Jung et al., 2015; Ramia et al., 2014). Fig. 4e also compares structures of the Cmr complex from *Sulfolobus islandicus* (SiCmr) in its apo, NTR- and CTR-bound forms. This work identified a critical change in Cmr3 called Stalk Loop that undergoes correlated changes when the cognate target RNA is bound, which is believed to play a role in opening or closing the cOA synthesis site (Sofos, 2020). Note that the Stalk Loop is a unique structural feature to the Cmr system.

To learn how Csm/Csx/NucC facilitate tandem detection through cOA-mediated enzyme activation, we also illustrate structures of Csm6 from *Thermococcus onnurineus* (ToCsm6 (Jia et al., 2019), Csx1 from *Sulfolobus islandicus* (SisCsx1) (Molina et al., 2019), and NucC from *Escherichia coli* (EcoNucC) (Lau et al., 2020), in their apo and cOA_n-bound forms and compare their RNase/DNase centers (Fig. 5). ToCsm6 forms a dimer with a single cOA_4 binding center while SiCsx1 forms a trimer of dimers with three cOA_4 binding centers (Fig. 5a) (Jia et al., 2019; Molina et al., 2019). Similar dimeric form was also observed in the cOA_6-bound EiCsm6 (Garcia-Doval et al., 2020). Thus, the RNase center is believed to be made of two HEPN domains, one from each protomer (Fig. 5a). Structural comparison shows that only minor structural changes are observed in HEPN when cOA is bound (Fig. 5a), unlike the changes observed in the HEPN domain of the activated Cas13 (Fig. 3). However, when comparing the structures of cOA_4 bound to HEPN active site likely mimicking ssRNA between an activated and an inactivated (W14A-E337A mutant) ToCsm, authors observed less optimal phosphodiester bond geometry for cleavage in the inactivated state (Fig. 5a) (Jia et al., 2019), suggesting a role of cOA_4 in promoting correct binding of RNA in the HEPN active site. Garcia-Doval *et al.* in studying the cOA_6-bound *Enteroccocus italicus* Csm6 (EiCsm6) proposed that it is possible that the HEPN domain may experience changes in dynamics when cOA_6 is bound, which could activate its RNase activity (Garcia-Doval et al., 2020). Alternatively, based on the observation that cOA_4 is bound in two different conformations in the three possible binding sites of the hexameric SisCsx1 complex (Fig. 5b), Molina et al. propose that the subtle changes in the hexamerization interface, especially with polar residues-mediated interactions, upon cOA_4 binding are sufficient to activate the RNase activity (Molina et al., 2019). Structural studies of EcoNucC further support the role of oligomerization in activation. NucC forms a trimer in absence of cOA_3 but a hexamer in presence of cOA_3, which is believed to facilitate binding of ds DNA substrates (Fig. 5c) (Lau et al., 2020).

Though other CARF-fused nucleases have not been repurposed for nucleic acid detection, mechanistic studies have revealed important insights. Structures of *Treponema succinifaciens* Card1 (TsuCard1) bound with cOA_4 reveals a conformational change-mediated metal coordination mechanism (Rostol, 2021) (Fig. 5d). Rostol *et al.* also provide an excellent discussion about other CARF-fused nucleases for further reading.

2. Summary

We summarize currently known structural properties of three CRISPR-Cas (or CRISPR-NucC hybrid) systems with a focus on the principle of how viral nucleic acids or second messengers stimulate collateral DNase/RNase activities. These remarkable properties have been exploited in constructing CRISPR-based nucleic acid detection methods. The systems outlined here seem to share the principle where a distantly bound stimulator can perturb the active site structures, through either enzyme oligomerization or protein dynamic changes. Confirmation of this principle requires additional biophysical studies and will open doors for more innovative nucleic acid detection methods.

Acknowledgements

The authors wish to thank the editors of JSB/JSB-X for an invitation to contribute to the annual collection with a Graphical Structural Biology Review (GRSB). This work was supported by NIH Grant R01 GM099604 to H.L.

References

Abudayyeh OO, et al. , 2016. C2c2 is a single-component programmable RNA-guided RNA-targeting CRISPR effector. Science.

Abudayyeh OO, Gootenberg JS, Essletzbichler P, Han S, Joung J, Belanto JJ, Verdine V, Cox DBT, Kellner MJ, Regev A, Lander ES, Voytas DF, Ting AY, Zhang F, 2017. RNA targeting with CRISPR-Cas13. Nature 550 (7675), 280–284. [PubMed: 28976959]

Abudayyeh OO, Gootenberg JS, Kellner MJ, Zhang F, 2019. Nucleic acid detection of plant genes using CRISPR-Cas13. CRISPR J 2 (3), 165–171. [PubMed: 31225754]

Ackerman CM, Myhrvold C, Thakku SG, Freije CA, Metsky HC, Yang DK, Ye SH, Boehm CK, Kosoko-Thoroddsen T-SF, Kehe J, Nguyen TG, Carter A, Kulesa A, Barnes JR, Dugan VG, Hung DT, Blainey PC, Sabeti PC, 2020. Massively multiplexed nucleic acid detection with Cas13. Nature 582 (7811), 277–282. [PubMed: 32349121]

Arizti-Sanz J, Freije CA, Stanton AC, Petros BA, Boehm CK, Siddiqui S, Shaw BM, Adams G, Kosoko-Thoroddsen T-S, Kemball ME, Uwanibe JN, Ajogbasile FV, Eromon PE, Gross R, Wronka L, Caviness K, Hensley LE, Bergman NH, MacInnis BL, Happi CT, Lemieux JE, Sabeti PC, Myhrvold C, 2020. Streamlined inactivation, amplification, and Cas13-based detection of SARS-CoV-2. Nat. Commun. 11 (1) 10.1038/s41467-020-19097-x.

Athukoralage JS, White MF, 2021. Cyclic oligoadenylate signalling and regulation by ring nucleases during type III CRISPR defence. RNA.

Barrangou R, 2015. The roles of CRISPR-Cas systems in adaptive immunity and beyond. Curr. Opin. Immunol. 32, 36–41. [PubMed: 25574773]

Barrangou R, Doudna JA, 2016. Applications of CRISPR technologies in research and beyond. Nat. Biotechnol. 34 (9), 933–941. [PubMed: 27606440]

Barrangou R, Marraffini L, 2014. CRISPR-Cas systems: prokaryotes upgrade to adaptive immunity. Mol. Cell 54 (2), 234–244. [PubMed: 24766887]

Chen JS, Ma E, Harrington LB, Da Costa M, Tian X, Palefsky JM, Doudna JA, 2018. CRISPR-Cas12a target binding unleashes indiscriminate single-stranded DNase activity. Science 360 (6387), 436–439. [PubMed: 29449511]

Cox DBT, Gootenberg JS, Abudayyeh OO, Franklin B, Kellner MJ, Joung J, Zhang F, 2017. RNA editing with CRISPR-Cas13. Science 358 (6366), 1019–1027. [PubMed: 29070703]

East-Seletsky A, O'Connell MR, Knight SC, Burstein D, Cate JHD, Tjian R, Doudna JA, 2016. Two distinct RNase activities of CRISPR-C2c2 enable guide-RNA processing and RNA detection. Nature 538 (7624), 270–273. [PubMed: 27669025]

Faure G, Shmakov SA, Yan WX, Cheng DR, Scott DA, Peters JE, Makarova KS, Koonin EV, 2019. CRISPR-Cas in mobile genetic elements: counter-defence and beyond. Nat. Rev. Microbiol. 17 (8), 513–525. [PubMed: 31165781]

Freije CA, Sabeti PC, 2021. Detect and destroy: CRISPR-based technologies for the response against viruses. Cell Host Microbe 29 (5), 689–703. [PubMed: 33915112]

Garcia-Doval C, Schwede F, Berk C, Rostøl JT, Niewoehner O, Tejero O, Hall J, Marraffini LA, Jinek M, 2020. Activation and self-inactivation mechanisms of the cyclic oligoadenylate-dependent CRISPR ribonuclease Csm6. Nat. Commun. 11 (1) 10.1038/s41467-020-15334-5.

Gootenberg JS, Abudayyeh OO, Lee JW, Essletzbichler P, Dy AJ, Joung J, Verdine V, Donghia N, Daringer NM, Freije CA, Myhrvold C, Bhattacharyya RP, Livny J, Regev A, Koonin EV, Hung DT, Sabeti PC, Collins JJ, Zhang F, 2017. Nucleic acid detection with CRISPR-Cas13a/C2c2. Science 356 (6336), 438–442. [PubMed: 28408723]

Gootenberg JS, Abudayyeh OO, Kellner MJ, Joung J, Collins JJ, Zhang F, 2018. Multiplexed and portable nucleic acid detection platform with Cas13, Cas12a, and Csm6. Science 360 (6387), 439–444. [PubMed: 29449508]

Gruschow S, Adamson CS, White MF, 2021. Specificity and sensitivity of an RNA targeting type III CRISPR complex coupled with a NucC endonuclease effector. Nucleic Acids Res.

Jia N, et al. , 2019. Type III-A CRISPR-Cas Csm complexes: assembly, periodic RNA cleavage, DNase activity regulation, and autoimmunity. Mol. Cell 73, 264–277 e265. [PubMed: 30503773]

Jia N, Jones R, Yang G, Ouerfelli O, Patel DJ, 2019. CRISPR-Cas III-A Csm6 CARF domain is a ring nuclease triggering stepwise cA4 cleavage with ApA>p formation terminating RNase activity. Mol. Cell 75, 944–956 e946. [PubMed: 31326273]

Jiang F, Doudna JA, 2017. CRISPR-Cas9 structures and mechanisms. Annu. Rev. Biophys. 46 (1), 505–529. [PubMed: 28375731]

Jung T-Y, An Y, Park K-H, Lee M-H, Oh B-H, Woo E, 2015. Crystal structure of the Csm1 subunit of the Csm complex and its single-stranded DNA-specific nuclease activity. Structure 23 (4), 782–790. [PubMed: 25773141]

Kazlauskiene M, Kostiuk G, Venclovas Č, Tamulaitis G, Siksnys V, 2017. A cyclic oligonucleotide signaling pathway in type III CRISPR-Cas systems. Science 357 (6351), 605–609. [PubMed: 28663439]

Knott GJ, East-Seletsky A, Cofsky JC, Holton JM, Charles E, O'Connell MR, Doudna JA, 2017. Guide-bound structures of an RNA-targeting A-cleaving CRISPR-Cas13a enzyme. Nat. Struct. Mol. Biol. 24 (10), 825–833. [PubMed: 28892041]

Lau RK, Ye Q, Birkholz EA, Berg KR, Patel L, Mathews IT, Watrous JD, Ego K, Whiteley AT, Lowey B, Mekalanos JJ, Kranzusch PJ, Jain M, Pogliano J, Corbett KD, 2020. Structure and mechanism of a cyclic trinucleotide-activated bacterial endonuclease mediating bacteriophage immunity. Mol. Cell 77 (4), 723–733.e6. [PubMed: 31932164]

Li S-Y, Cheng Q-X, Wang J-M, Li X-Y, Zhang Z-L, Gao S, Cao R-B, Zhao G-P, Wang J, 2018. CRISPR-Cas12a-assisted nucleic acid detection. Cell Discov. 4 (1) 10.1038/s41421-018-0028-z.

Li L, Li S, Wu N.a., Wu J, Wang G, Zhao G, Wang J, 2019. HOLMESv2: A CRISPR-Cas12b-assisted platform for nucleic acid detection and DNA methylation quantitation. ACS Synth. Biol. 8 (10), 2228–2237. [PubMed: 31532637]

Liu TY, Knott GJ, Smock DCJ, Desmarais JJ, Son S, Bhuiya A, Jakhanwal S, Prywes N, Agrawal S, Díaz de León Derby M, Switz NA, Armstrong M, Harris AR, Charles EJ, Thornton BW, Fozouni P, Shu J, Stephens SI, Kumar GR, Zhao C, Mok A, Iavarone AT, Escajeda AM, McIntosh R, Kim S, Dugan EJ, Hamilton JR, Lin-Shiao E, Stahl EC, Tsuchida CA, Moehle EA, Giannikopoulos P, McElroy M, McDevitt S, Zur A, Sylvain I, Ciling A, Zhu M, Williams C, Baldwin A, Pollard KS, Tan MX, Ott M, Fletcher DA, Lareau LF, Hsu PD, Savage DF, Doudna JA, 2021. Accelerated RNA detection using tandem CRISPR nucleases. Nat. Chem. Biol. 17 (9), 982–988. [PubMed: 34354262]

Liu L, Li X, Wang J, Wang M, Chen P, Yin M, Li J, Sheng G, Wang Y, 2017. Two distant catalytic sites are responsible for C2c2 RNase activities. Cell 168 (1–2), 121–134.e12. [PubMed: 28086085]

Liu L, Li X, Ma J, Li Z, You L, Wang J, Wang M, Zhang X, Wang Y, 2017. The molecular architecture for RNA-guided RNA cleavage by Cas13a. Cell 170 (4), 714–726.e10. [PubMed: 28757251]

Makarova KS, et al. , 2020. Evolutionary classification of CRISPR-Cas systems: a burst of class 2 and derived variants. Nat. Rev. Microbiol. 18, 67–83. [PubMed: 31857715]

Makarova KS, Zhang F, Koonin EV, 2017. SnapShot: class 1 CRISPR-Cas systems. Cell 168, 946–946 e941. [PubMed: 28235204]

Makarova KS, Zhang F, Koonin EV, 2017. SnapShot: class 2 CRISPR-Cas systems. Cell 168, 328–328 e321. [PubMed: 28086097]

Molina R, Stella S, Feng M, Sofos N, Jauniskis V, Pozdnyakova I, López-Méndez B, She Q, Montoya G, 2019. Structure of Csx1-cOA4 complex reveals the basis of RNA decay in Type III-B CRISPR-Cas. Nat. Commun. 10 (1) 10.1038/s41467-019-12244-z.

Molina R, Sofos N, Montoya G, 2020. Structural basis of CRISPR-Cas Type III prokaryotic defence systems. Curr. Opin. Struct. Biol. 65, 119–129. [PubMed: 32712502]

Niewoehner O, Garcia-Doval C, Rostøl JT, Berk C, Schwede F, Bigler L, Hall J, Marraffini LA, Jinek M, 2017. Type III CRISPR-Cas systems produce cyclic oligoadenylate second messengers. Nature 548 (7669), 543–548. [PubMed: 28722012]

Nishimasu H, Yamano T, Gao L, Zhang F, Ishitani R, Nureki O, 2017. Structural basis for the altered PAM recognition by engineered CRISPR-Cpf1. Mol. Cell 67 (1), 139–147.e2. [PubMed: 28595896]

Ramia NF, Tang L, Cocozaki AI, Li H, 2014. Staphylococcus epidermidis Csm1 is a 3'-5' exonuclease. Nucl. Acids Res. 42 (2), 1129–1138. [PubMed: 24121684]

Rostol JT, et al. , 2021. The Card1 nuclease provides defence during type III CRISPR immunity. Nature 590, 624–629. [PubMed: 33461211]

Santiago-Frangos A, Hall LN, Nemudraia A, Nemudryi A, Krishna P, Wiegand T, Wilkinson RA, Snyder DT, Hedges JF, Cicha C, Lee HH, Graham A, Jutila MA, Taylor MP, Wiedenheft B, 2021. Intrinsic signal amplification by type III CRISPR-Cas systems provides a sequence-specific SARS-CoV-2 diagnostic. Cell Rep. Med. 2 (6), 100319. 10.1016/j.xcrm.2021.100319. [PubMed: 34075364]

Smargon AA, Cox DBT, Pyzocha NK, Zheng K, Slaymaker IM, Gootenberg JS, Abudayyeh OA, Essletzbichler P, Shmakov S, Makarova KS, Koonin EV, Zhang F, 2017. Cas13b Is a type VI-B CRISPR-associated RNA-guided RNase differentially regulated by accessory proteins Csx27 and Csx28. Mol. Cell 65 (4), 618–630.e7. [PubMed: 28065598]

Sofos N, et al. , 2020. Structures of the Cmr-beta complex reveal the regulation of the immunity mechanism of type III-B CRISPR-Cas. Mol. Cell 79, 741–757 e747. [PubMed: 32730741]

Sorek R, Lawrence CM, Wiedenheft B, 2013. CRISPR-mediated adaptive immune systems in bacteria and archaea. Annu. Rev. Biochem. 82 (1), 237–266. [PubMed: 23495939]

Sridhara S, et al. , 2021. Structure and function of an in vivo assembled type III-A CRISPR-Cas complex reveal critical roles of dynamics in activity control. bioRxiv.

Sridhara S, Goswami HN, Whyms C, Dennis JH, Li H, 2021. Virus detection via programmable Type III-A CRISPR-Cas systems. Nat. Commun. 12, 5653. [PubMed: 34580296]

Steens JA, Zhu Y, Taylor DW, Bravo JPK, Prinsen SHP, Schoen CD, Keijser BJF, Ossendrijver M, Hofstra LM, Brouns SJJ, Shinkai A, van der Oost J, Staals RHJ, 2021. SCOPE enables type III CRISPR-Cas diagnostics using flexible targeting and stringent CARF ribonuclease activation. Nat. Commun. 12 (1) 10.1038/s41467-021-25337-5.

Stella S, Alcón P, Montoya G, 2017. Class 2 CRISPR-Cas RNA-guided endonucleases: Swiss Army knives of genome editing. Nat. Struct. Mol. Biol. 24 (11), 882–892. [PubMed: 29035385]

Stella S, Alcón P, Montoya G, 2017. Structure of the Cpf1 endonuclease R-loop complex after target DNA cleavage. Nature 546 (7659), 559–563. [PubMed: 28562584]

Stella S, Mesa P, Thomsen J, Paul B, Alcón P, Jensen SB, Saligram B, Moses ME, Hatzakis NS, Montoya G, 2018. Conformational activation promotes CRISPR-Cas12a catalysis and resetting of the endonuclease activity. Cell 175 (7), 1856–1871. e21. [PubMed: 30503205]

Swarts DC, Jinek M, 2018. Cas9 versus Cas12a/Cpf1: Structure-function comparisons and implications for genome editing. Wiley interdisciplinary reviews. RNA 9 (5). 10.1002/wrna.2018.9.issue-510.1002/wrna.1481.

Swarts DC, van der Oost J, Jinek M, 2017. Structural basis for guide RNA processing and seed-dependent DNA targeting by CRISPR-Cas12a. Mol. Cell 66 (2), 221–233.e4. [PubMed: 28431230]

Wang L, Mo CY, Wasserman MR, Rostøl JT, Marraffini LA, Liu S, 2019. Dynamics of Cas10 govern discrimination between self and non-self in type III CRISPR-Cas immunity. Mol. Cell 73 (2), 278–290.e4. [PubMed: 30503774]

Wang D, Zhang F, Gao G, 2020. CRISPR-based therapeutic genome editing: strategies and in vivo delivery by AAV vectors. Cell 181, 136–150. [PubMed: 32243786]

Wang B, Zhang T, Yin J, Yu Y, Xu W, Ding J, Patel DJ, Yang H, 2021. Structural basis for self-cleavage prevention by tag:anti-tag pairing complementarity in type VI Cas13 CRISPR systems. Mol. Cell 81 (5), 1100–1115.e5. [PubMed: 33472057]

Wright A, Nuñez J, Doudna J, 2016. Biology and applications of CRISPR systems: harnessing nature's toolbox for genome engineering. Cell 164 (1–2), 29–44. [PubMed: 26771484]

Yamano T, Zetsche B, Ishitani R, Zhang F, Nishimasu H, Nureki O, 2017. Structural basis for the canonical and non-canonical PAM recognition by CRISPR-Cpf1. Mol. Cell 67 (4), 633–645.e3. [PubMed: 28781234]

Yang H, Gao P.u., Rajashankar KR, Patel DJ, 2016. PAM-dependent target DNA recognition and cleavage by C2c1 CRISPR-Cas endonuclease. Cell 167 (7), 1814–1828.e12. [PubMed: 27984729]

You L, et al. , 2019. Structure studies of the CRISPR-Csm complex reveal mechanism of co-transcriptional interference. Cell 176, 239–253 e216. [PubMed: 30503210]

Zetsche B, Heidenreich M, Mohanraju P, Fedorova I, Kneppers J, DeGennaro EM, Winblad N, Choudhury SR, Abudayyeh OO, Gootenberg JS, Wu WY, Scott DA, Severinov K, van der Oost J, Zhang F, 2017. Multiplex gene editing by CRISPR-Cpf1 using a single crRNA array. Nat. Biotechnol. 35 (1), 31–34. [PubMed: 27918548]

Zhang F, 2019. Development of CRISPR-Cas systems for genome editing and beyond. Q. Rev. Biophys. 52 (E6).

Zhang C, Konermann S, Brideau NJ, Lotfy P, Wu X, Novick SJ, Strutzenberg T, Griffin PR, Hsu PD, Lyumkis D, 2018. Structural basis for the RNA-guided Ribonuclease activity of CRISPR-Cas13d. Cell 175 (1), 212–223.e17. [PubMed: 30241607]

Zhang H, Li Z, Xiao R, Chang L, 2020. Mechanisms for target recognition and cleavage by the Cas12i RNA-guided endonuclease. Nat. Struct. Mol. Biol. 27 (11), 1069–1076. [PubMed: 32895556]

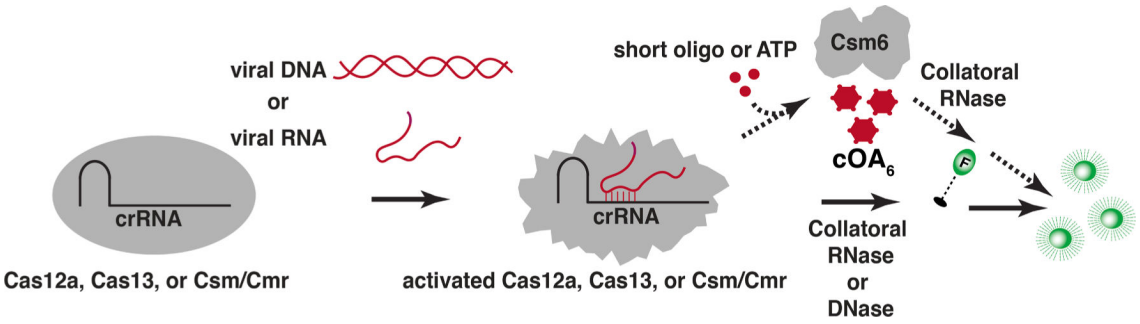

Fig. 1.

Schematic of how Clustered Regularly Interspaced Short Palindromic Repeat (CRISPR) and CRISPR-associated (Cas) (CRISPR-Cas) enzymes are activated by either viral DNA or RNA and how this property is repurposed for specific detection of nucleic acids. In addition to the interference activity towards the viral DNA and RNA directly, certain CRISPR-Cas enzymes elicit collateral deoxyribonuclease (DNase) or ribonuclease (RNase) activities that are harnessed to cleave fluorescence reporter molecules. The Type III CRISPR-Cas enzymes also possess RNA-activated cyclic oligoadenylate (cOA) synthesis activity that is harnessed to stimulate the ancillary cOA sensor molecules (Csm6, Csx1, or NucC) that further amplify fluorescence signals.

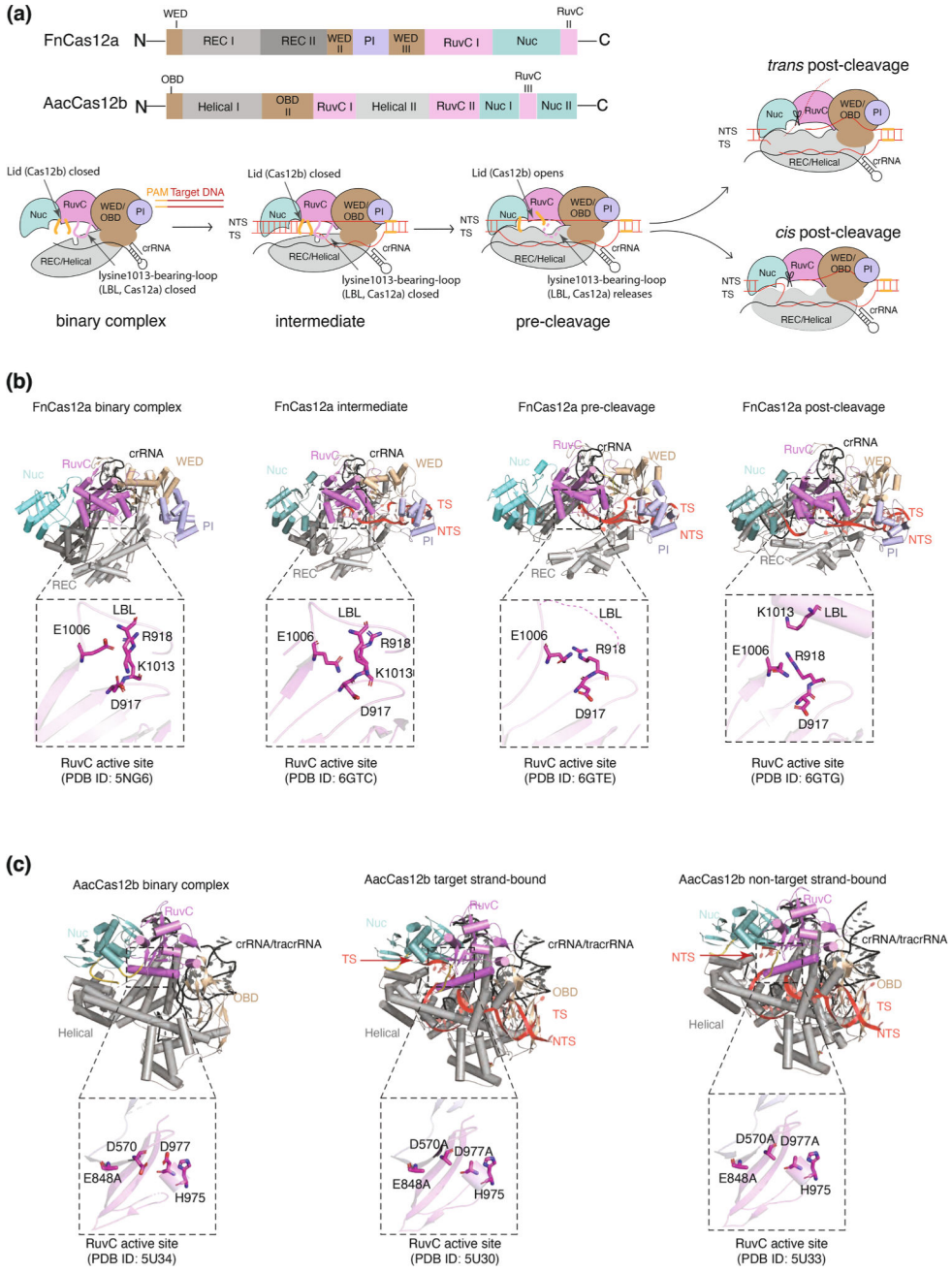

Fig. 2.

Structural comparison of two Cas12 enzymes in the absence or presence of the target DNA reveals rearranged catalytic sites upon target DNA binding. Domains and nucleic acids are colored consistently throughout the figure. The crRNA and tracrRNA are colored in black and the target DNA is in red. The displayed Cas12 structures are orientated identically with their nuclease domain (Nuc) superimposed. PDB ID for each complex is indicated. Insets show close-up view of the catalytic site structure in various Cas12a/Cas12b complexes. (a) Domain organization of *Francisella novicida* Cas12a (FnCas12a) and *Alicyclobacillus acidoterrestris* Cas12b (AacCas12b) and a model of the DNA stimulated catalytic processes.

Each domain is colored in the same scheme as the linear organization bar diagram. Key features with respect to the activation processes are noted on top of the cartoons. Cas12a consists of five domains in total: a nuclease domain (Nuc), a nucleic acid recognition domain (REC, gray), a wedge domain (WED, wheat), a PAM interaction domain (PI, light blue), and a DNase domain (RuvC, violet). Cas12b contains the same except for the WED and PI are replaced by the oligo nucleotide binding domain (OBD) and REC is replaced by the Helical domain. The Cas12a/Cas12b-CRISPR RNA (crRNA, black) complex acts as a surveillance complex with the unpaired guide region of crRNA resting on the REC domain. Upon binding to the complementary target DNA (red) containing a protospacer associated motif (PAM, yellow), the guide-target heteroduplex rearranges the REC domain, leading to activation of the catalytic RuvC domain. The activated Cas12a/Cas12b cleaves any DNA non-specifically in the vicinity (*trans*-cleavage) including the bound target DNA (*cis*-cleavage). (b) Cartoon representation and close-up active site views of the FnCas12a in multiple functional states: binary (crRNA-bound), intermediate, pre-cleavage and post cleavage ternary complex captured by cryoEM studies. The catalytic residues in FnCas12a, Asp917, Glu1006 (mutated to Gln1006) and two positively charged residues, Lys1013 and Arg918, are shown in stick models. The loop harboring Lys1013 is named lysine1013-bearing-loop (LBL) and undergoes large re-arrangement from the pre-cleavage to the post-cleavage state. This re-re-arrangement plays an important role in freeing up the catalytic residues Asp917 and Glu1006 to form the active site. (b) Cartoon representation and close-up active site views of the AacCas12b in multiple functional states: binary (crRNA- and tracrRNA-bound), target strand-bound ternary complex and non-target strand-bound ternary complex captured by crystallographic studies. The DNase domain RuvC remains relatively stationary from DNA-free, to target strand-bound and to non-target strand-bound. Two loops in front of the active site (Lid) are closed in the DNA-free form but open when either DNA strand is bound.

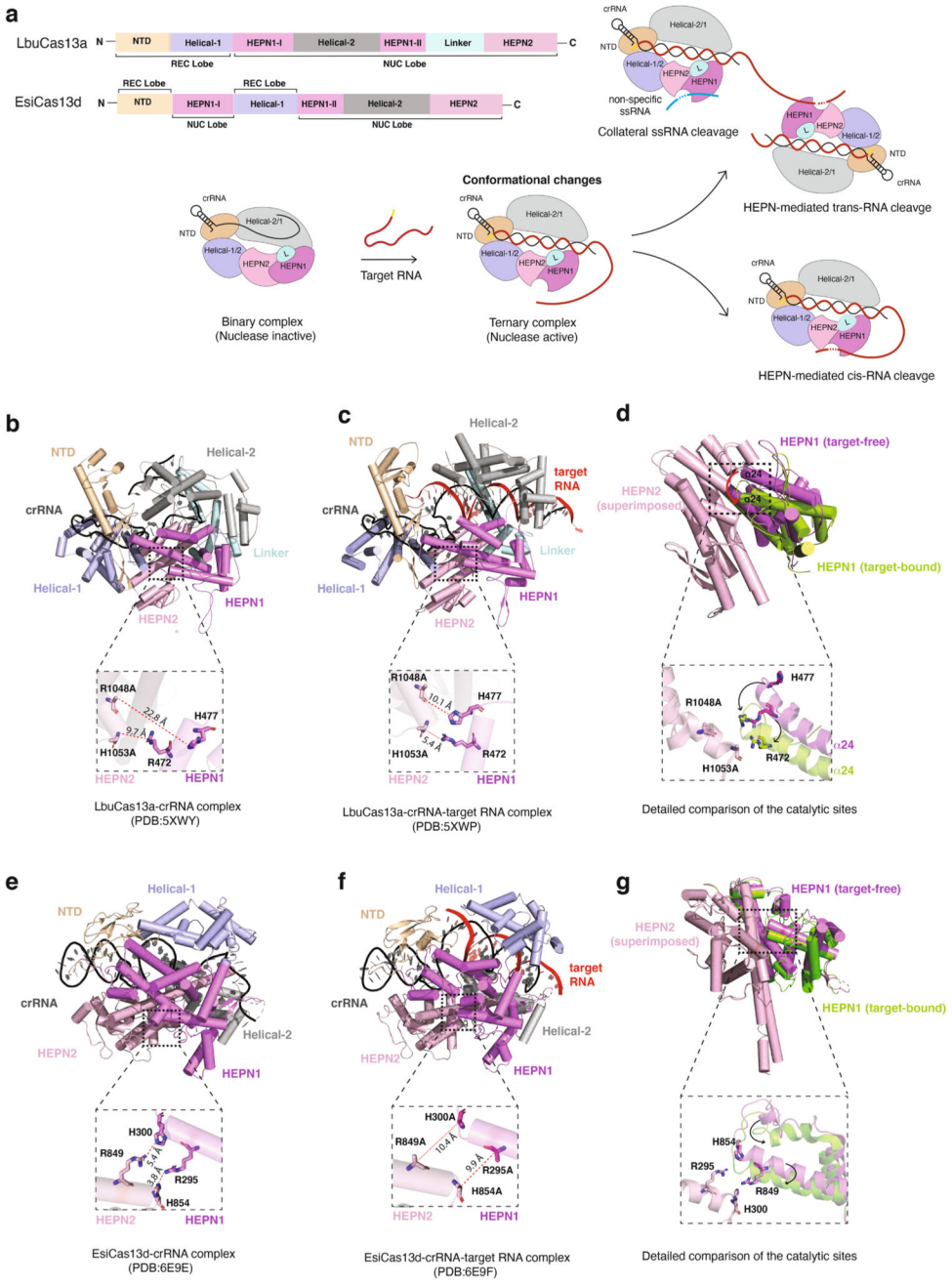

Fig. 3.

Structure comparison of two Cas13 enzymes in the absence or presence of the target RNA reveals rearranged catalytic sites upon target RNA binding. Domains and RNA are colored consistently throughout the figure. The displayed Cas13 structures are oriented identically with their HEPN2 domain superimposed. PDB ID for each complex is indicated. Insets show close-up view of the catalytic site structure in various Cas13a/Cas13d complexes. Distances are measured between the sidechains of two catalytic (or mutant) residues. (a) Domain organization of *Leptotrichia buccalis* Cas13a (LbuCas13a) and *Eubacterium siraeum* Cas13d (EsiCas13d) and a model of crRNA-guided target-RNA cleavage by Cas13.

Cas13a consists of six domains in total: N-terminal domain (wheat), Helical-1 (light blue), Helical-2 (gray), HEPN1 (violet) and HEPN2 (light pink) and Linker (pale cyan) domain. The more compact Cas13d contains the same except for the Linker domain arranged in a different linear sequence order. The Cas13a/Cas13d-CRISPR RNA (crRNA, black) complex acts as a surveillance complex with the unpaired guide region of crRNA resting on Helical 2 (Cas13a) or Helical 1 (Cas13d) domain. Upon binding to the complementary target RNA (red) containing a non-complementary 3' protospacer flanking sequence (3' PFS, yellow), the guide-target duplex rearranges the Helical and the HEPN domains, leading to formation of the catalytic site as the HEPN1 domain comes closer to the HEPN2 domain. The activated Cas13a/Cas13d cleaves any RNA non-specifically in the vicinity (*trans*-cleavage) including the bound target RNA 5' distal to the complementary region (*cis*-cleavage). Two possible modes of *trans*-cleavage are illustrated. (b) Cartoon representation of the LbuCas13a-crRNA binary complex and close-up view of the active site. (c) Cartoon representation of the LbuCas13a-crRNA-target RNA ternary complex and close-up view of the active site indicate a more compact active site. (d) Movement of the HEPN1 domain relative to the HEPN2 domain upon target RNA binding in both cartoon representation and close-up view. (e) Cartoon representation of the EsiCas13d-crRNA binary complex and close-up view of the active site. (f) Cartoon representation of the EsiCas13d-crRNA-target RNA ternary complex and close-up view of the active site indicate a more compact active site. Note the mutations in the active site. (g) Movement of the HEPN1 domain relative to the HEPN2 domain upon target RNA binding in both cartoon representation and close-up view.

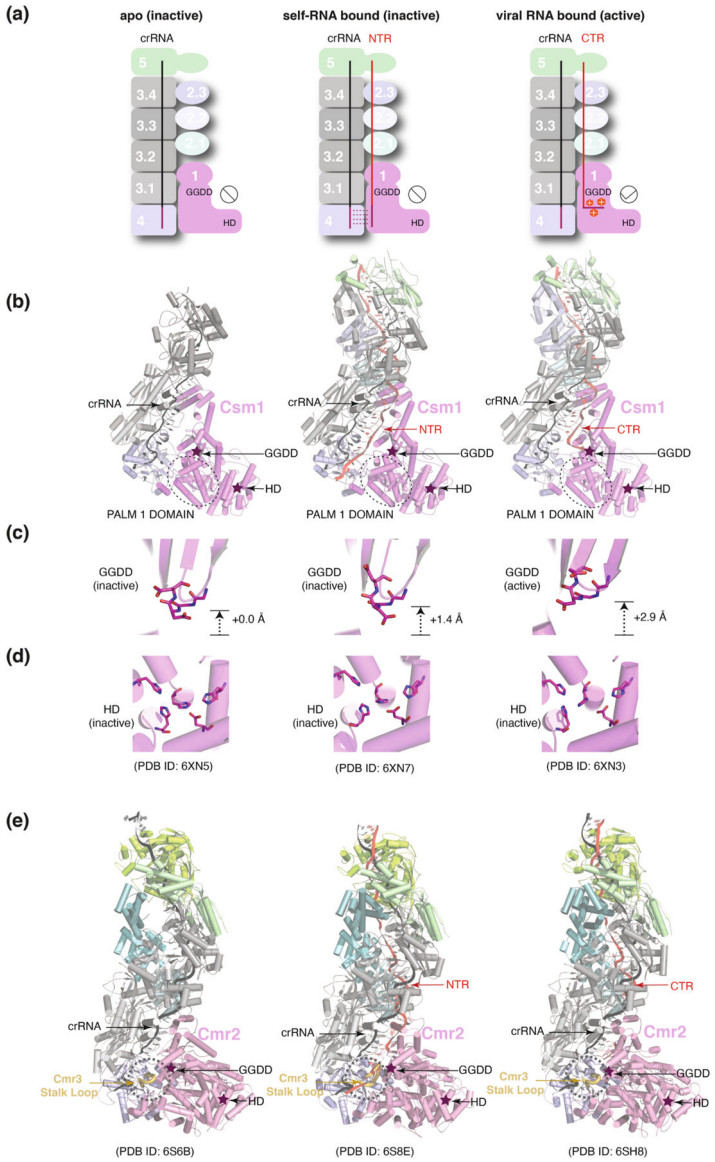

Fig. 4.

Structure comparison of the Type III CRISPR-Cas enzymes in the apo, self-RNA-bound (noncognate RNA target, or NTR), and the viral RNA-bound (cognate RNA target, or CTR) states indicates rearrangement of the cyclic oligonucleotide (cOA) synthesis site (GGDD motif) but minor changes in the DNase site (HD domain). Domains and RNA are colored consistently throughout the figure. CRISPR RNA (crRNA) is in black, and the target RNA is in red. The displayed Csm (III-A) and Cmr (III-B) structures are orientated identically with their PALM1 of the Csm1/Cmr2 subunit superimposed. PDB ID for each complex is indicated. (a) Schematic assemblies of the Csm/Cmr complexes in apo, NTR-bound and CTR-bound forms as observed by cryo-electron microscopy (cryoEM). Corresponding subunits represented by colored solids are labeled. The two catalytic sites are labeled by GGDD for the cOA_n (n = 3, 4, 5, or 6) synthesis and HD for the deoxyribonuclease (DNase) site, respectively; (b) Cartoon representation of the cryoEM structures for the *Lactococcus*

lactis Csm (LlCsm) with the two catalytic sites and other key elements labeled. The PALM 1 domain is circled; (c) Viral RNA activates cOA_6 synthesis activity of LlCsm through opening the GGDD active site. Comparison of the GGDD active site in the apo, the NTR-bound, and the CTR-bound forms when all three structures are aligned using their PALM 1 domain. In comparison with the GGDD catalytic loop, that in the NTR-bound moved up by 1.4 Å while that in the CTR-bound moved up by 2.9 Å. (d) The DNase active site of LlCsm undergoes minor change in different functional forms. Comparison of the HD active site in the apo, the NTR-bound, and the CTR-bound forms when all three structures are aligned using their PALM 1 domain. It has been proposed that the viral RNA-activated DNase is a result of dynamic changes in the HD domain. (e) Cartoon representation of the cryoEM structures of the *Sulfolobus islandicus* Cmr (SisCmr) with the two catalytic sites and other key elements labeled. Unlike LlCsm, SisCmr uses the Stalk Loop of its Cmr3 subunit as a sensor to trigger changes in the cOA_n synthesis site (GGDD) upon CTR binding. Like LlCsm, while the HD site itself undergoes minimal changes, those in surrounding loops accompanying protein dynamics changes could explain activation of the DNase activity.

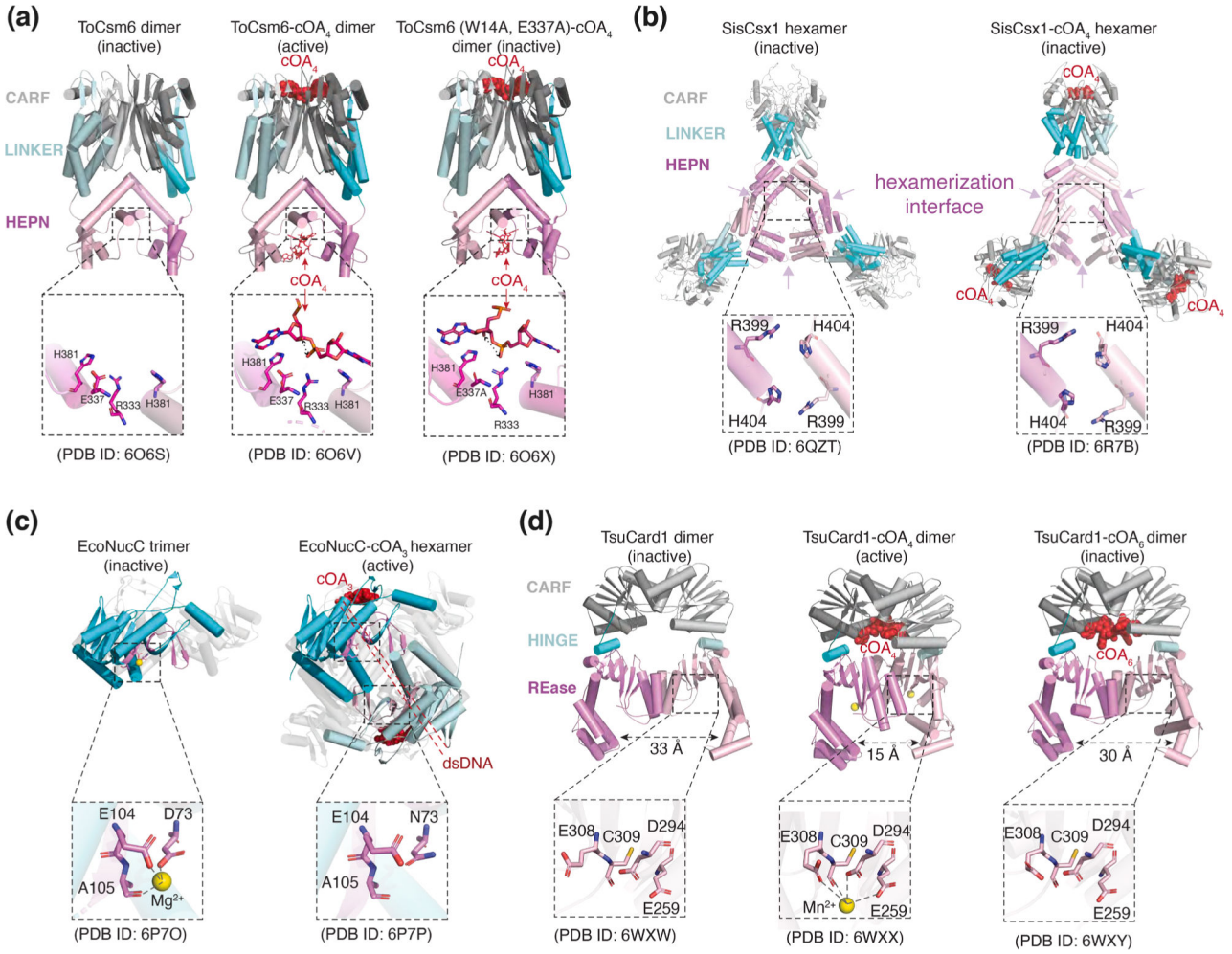

Fig. 5.

Structural comparison of Csm6, NucC, and Card1 in absence or presence of cyclic oligoadenylates (cOA_n where n = 3, 4 or 6) reveals rearranged catalytic sites upon cOA_n binding. Domains are colored consistently throughout the figure. The displayed Csm6/NucC/Card1 structures are orientated identically with one of their respective catalytic domains superimposed. PDB ID for each complex is indicated. Insets show close-up view of the catalytic site structure in various Csm6/NucC/Card1 complexes. (a) Cartoon representation of *Thermococcus onnurineus* Csm6 (ToCsm6) in absence and presence of cOA_4 and close-up views of the active sites. The three domains, CARF, LINKER, and HEPN are labeled and colored in two different shades for the two protomers. The composite active site is formed by both HEPN domains of the homodimer, and in presence of cOA_4, both the CARF and HEPN sites of ToCsm6 are bound with the ligand. Though the geometry of the active site has only minor changes, the sugar phosphate backbone of cOA_4 bound to ToCsm6 HEPN differs between the activated (wild-type) and the inactivated (W14A-E337) form, which implies that single stranded RNA substrates interact with the catalytic residues differently when ToCsm is activated by cOA_4. (b) Cartoon representation of *Sulfolobus islandicus* Csx1 (SisCsx1) in absence and presence of cOA_4 and close-up views of active sites. The three domains, CARF, LINKER, and HEPN are labeled and colored in two

different shades for each dimer subunit. While most Csm6 seem to form a dimer, SisCsx1 forms a hexamer regardless of whether it is bound to cOA_4. It is believed that cOA_4 binding alters the oligomerization interfaces (pink arrows) that allosterically activate the three composite enzymatic centers to cleave RNA. (c) Cartoon representation of *Escherichia coli* NucC (EcoNucC) in absence and presence of cOA_4 and close-up views of the active sites. The ß-strands carrying the catalytic residues are colored in pink and the rest is in cyan. Significantly, cOA_3-free NucC is a trimer while cOA_3-bound NucC is a hexamer, which facilitates its DNase activity by forming an extended DNA binding surface with a pair of active sites. The active site residue Asp73 was mutated to asparagine, which led to the loss of the bound Mg^{2+}. (d) Cartoon representation of *Treponema succinifaciens* Card1 (TsuCard1) in absence and presence of the activating cOA_4 or deactivating cOA_6 and close-up views of the active sites. The three domains, CARF, LINKER, and REase (Restriction Endonuclease), are labeled and colored in two different shades for each dimer subunit. Significantly, the cOA_4-free or cOA_6-bound TsuCard1 dimer has a wide separation between the two REase domains that is compacted by the binding of cOA_4 with a slightly rearranged active site for binding the catalytic Mn^{2+}.